Hindawi Publishing Corporation
Active and Passive Electronic Components
Volume 2011, Article ID 284767, 7 pages
doi:10.1155/2011/284767

Research Article

A K-Band RF-MEMS-Enabled Reconfigurable and Multifunctional Low-Noise Amplifier Hybrid Circuit

R. Malmqvist,[1,2] C. Samuelsson,[1] A. Gustafsson,[1] P. Rantakari,[3] S. Reyaz,[2] T. Vähä-Heikkilä,[3] A. Rydberg,[2] J. Varis,[3] D. Smith,[4] and R. Baggen[5]

[1] *Department of Subsystems Technology, Swedish Defence Research Agency (FOI), SE-58330 Linköping, Sweden*
[2] *Department of Engneering Sciences, Uppsala University, SE-75105 Uppsala, Sweden*
[3] *VTT Technical Research Centre of Finland, FI-02044 VTT, Espoo, Finland*
[4] *OMMIC S.A.S., 94453 Limeil-Brèvannes Cedex, France*
[5] *Department of Antennas and EM-Modelling, IMST GmbH, D-47475 Kamp-Lintfort, Germany*

Correspondence should be addressed to R. Malmqvist, robert.malmqvist@foi.se

Received 11 July 2011; Accepted 31 August 2011

Academic Editor: Jiun Wei Horng

A K-band (18–26.5 GHz) RF-MEMS-enabled reconfigurable and multifunctional dual-path LNA hybrid circuit (optimised for lowest/highest possible noise figure/linearity, resp.) is presented, together with its subcircuit parts. The two MEMS-switched low-NF (higher gain) and high-linearity (lower gain) LNA circuits (paths) present 16.0 dB/8.2 dB, 2.8 dB/4.9 dB and 15 dBm/20 dBm of small-signal gain, noise figure, and 1 dB compression point at 24 GHz, respectively. Compared with the two (fixed) LNA subcircuits used within this design, the MEMS-switched LNA circuit functions show minimum 0.6–1.3 dB higher NF together with similar values of $P_{1\,\mathrm{dB}}$ at 18–25 GHz. The gain of one LNA circuit path is reduced by 25–30 dB when the MEMS switch and active circuitry used within in the same switching branch are switched off to select the other LNA path and minimise power consumption.

1. Introduction

High-performance RF switches and switch circuits are key elements in wireless applications related to communication and sensing systems. Solid-state switches using transistors or diodes are commonly used in such applications, but they are rather narrow-band, nonlinear and have relatively high losses at microwave and millimetre-wave frequencies [1, 2]. RF-micro-electro-mechanical-system (MEMS) switches have recently emerged as a potential option for replacing them in switching circuits for certain applications because of their superior RF performance for wideband/multiband operation (e.g., switches from RadantMEMS) [3]. This is important, for example, in low-noise receivers where the losses before the first amplification stage, that is, the low-noise amplifier (LNA) will have an impact on the overall noise figure (NF). Reconfigurable high-performance (low loss/DC power and high isolation/linearity) front-ends are needed in RF systems such as wireless communication/space/aerospace applications within the microwave/mm wave range. Most of the research work carried out to this date, however, has lacked much real demonstration of a successful integration of active RF circuits and MEMS switches, especially at frequencies above 10 GHz.

RF-MEMS together with active circuitry (such as low-noise/power amplifiers) have with a few notable exceptions mainly been realised up to 5–10 GHz (see, e.g., [4–14]) which still leaves room for significant improvements to be made with respect to RF performance, frequency range, and functionality as well as to achieve reduced complexity and lower costs. Measured *s*-parameter data of a 26–30 GHz MEMS-switched transmit/receive circuit was reported in [5]. However, the noise figure and linearity of the MEMS switched LNA subpart were not presented in this case. In this paper, we present the results of a K-band (18–26.5 GHz) reconfigurable and multifunctional (low-NF and high-linearity) LNA hybrid circuit that has been realised using a dual-LNA GaAs MMIC combined with an RF-MEMS single-pole-double-throw (SPDT) switch network made on a quartz substrate (a block circuit schematic is depicted in Figure 1).

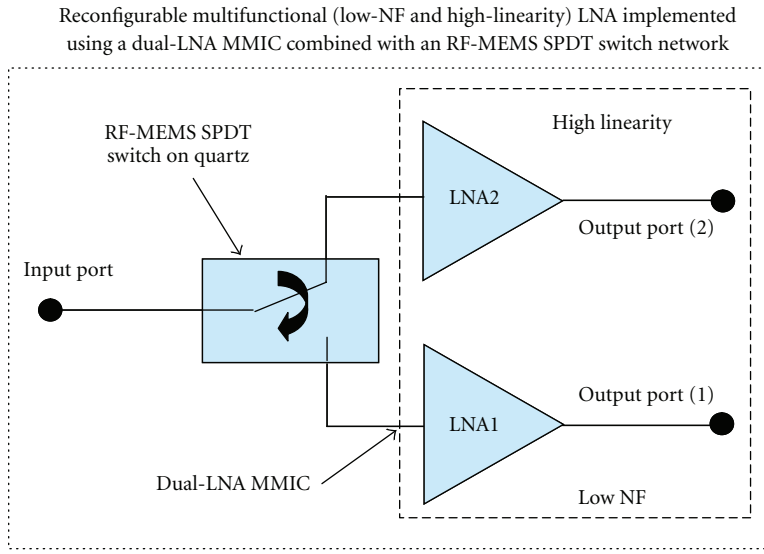

Figure 1: Schematic of an RF-MEMS enabled reconfigurable and multifunctional (low-NF and high-linearity) dual-path LNA (with LNA circuit functions denoted as LNA1 and LNA2, resp.).

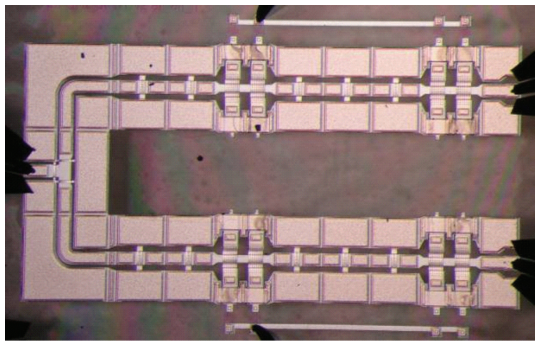

Figure 2: A photograph of a K-band RF-MEMS SPDT switch network fabricated on a quartz substrate (VTT process).

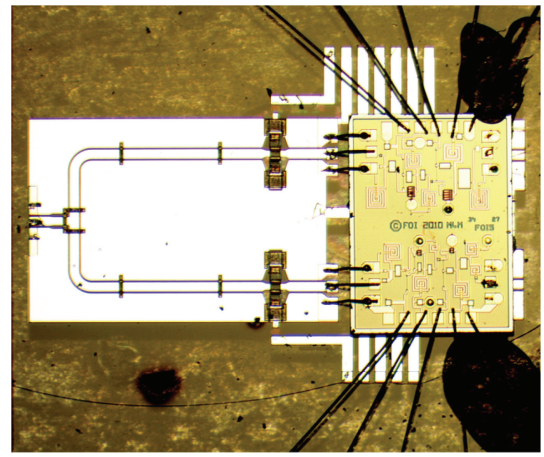

Figure 3: A photograph of a K-band reconfigurable (multifunctional) LNA hybrid circuit realised using a MEMS SPDT switch network (to the left) wire-bonded to a dual-LNA GaAs MMIC (to the right) designed for low NF and high linearity, respectively.

The dual-LNA MMIC contains two LNAs optimised for low noise and high linearity, respectively. The reconfigurable MEMS dual-LNA may also be integrated with different downconverter stages (selected for lowest possible NF or highest possible dynamic range) into complete wideband (or multiband) front-ends. Small- and large-signal data of the reconfigurable MEMS K-band LNA device (including also the subcircuit parts) will be presented next.

2. Reconfigurable/Multifunctional K-Band LNA

2.1. RF-MEMS SPDT Switch Networks and Dual-LNA MMIC. Figure 2 shows a photograph of a K-band SPDT switch network that has been fabricated on a fused silica (quartz) substrate using a capacitive RF-MEMS process at VTT [14]. It is composed of a power divider and capacitive MEMS shunt switches. The MEMS switches were used in pairs to enhance the isolation between the ports. The distance between the switches and the distance from the power divider were optimised for maximum RF performance in terms of isolation, insertion loss, and impedance matching. When the switches at one of the output ports (e.g., Output 1) are open (ON state) and the switches at the other output port (Output 2) are closed (OFF state), the RF input power is connected to Output 1 and vice versa. The SPDT switch network was controlled by applying a control voltage of 45 V to the MEMS switches. As the bias circuit only has to provide an electrostatic field, the DC power consumption (P_{DC}) is extremely low and only a small leakage current will flow (<5–10 μA). Figure 4(a) shows measured and simulated s-parameters of the SPDT switch shown in Figure 2. The s-parameter data was measured using a probe station (with all RF ports terminated with 50 Ω) and an Agilent PNA E8361A network analyzer which was calibrated using on-wafer calibration standards. For the MEMS SPDT circuit shown in Figure 2, the measured ON/OFF state s_{21}/s_{31}

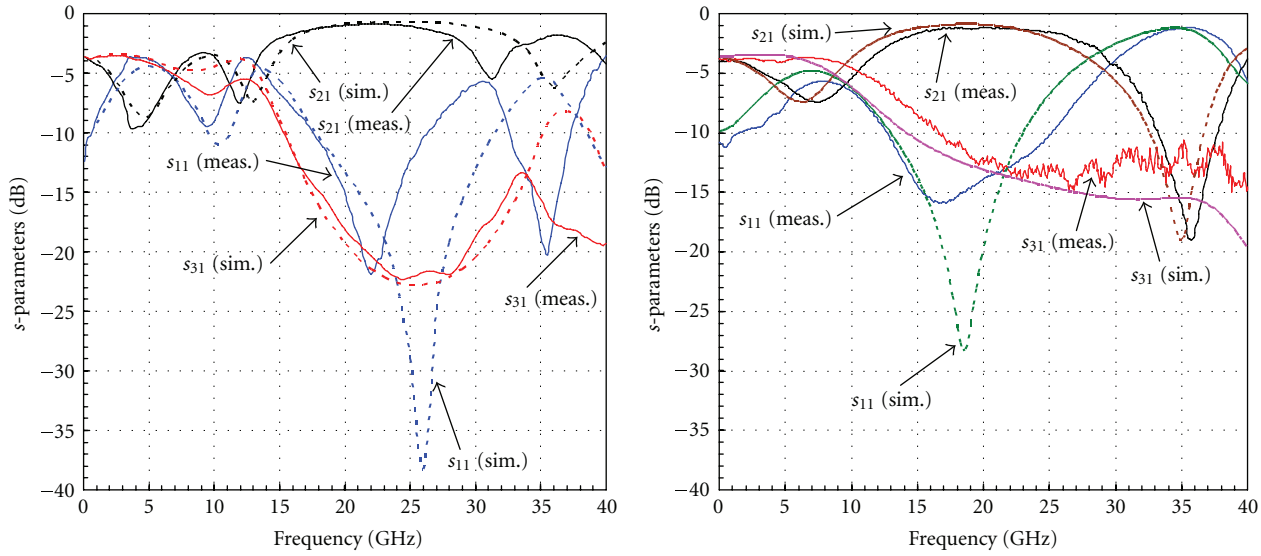

FIGURE 4: Measured and simulated *s*-parameters of two types of SPDT switch networks realised using (a) several MEMS switches and (b) a single MEMS switch within each switching branch, respectively.

(transmission/isolation) and s_{11} (input matching) equal -0.9 dB/-20 dB and -22 dB at 22 GHz, respectively. The measured s_{11} resonance peak occurred at a somewhat lower centre frequency than simulated which could be due to the realised MEMS switch air gaps being slightly smaller than expected (and thus resulting in an increased capacitive loading of the SPDT switch network). Figure 3 shows a photograph of a K-band reconfigurable LNA hybrid circuit realised using a similar type of MEMS SPDT switch network made on quartz (shown to the left) that was wire bonded to a dual-LNA GaAs MMIC (to the right). A single MEMS switch was used in each branch to reduce dimensions and complexity. The two SPDT switches shown in Figures 2 and 3 have circuit areas of 5×3 mm^2.

Figure 4(b) shows the corresponding *s*-parameter data of the SPDT circuit shown in Figure 3 (measured before wire bonding). The measured results show that this SPDT switch circuit is well matched around 15–20 GHz (with a minimum insertion loss of 1.2 dB and 12 dB of isolation at 20 GHz, resp.). Compared with simulations, this is occurring in a frequency band which is a few GHz lower than expected and the in-band insertion loss was found to be some tenths of a dB higher than simulated (see Figure 4(b)). The frequency shift may be explained by an increased capacitive loading of the different air bridges used on top of the coPlanar Waveguide (CPW) transmission lines (see Figure 2). A possible reason for this to occur may be due to a remaining sacrificial layer that was not completely removed under the ground plane interconnects (since no release holes were made on those structures) something that will result in a higher effective dielectric constant (than air) and thus also a higher capacitive load.

The *s*-parameter data of the MEMS LNA hybrid circuit (including also its active/passive subcircuit parts) was measured from 5 GHz/10 MHz up to 40 GHz using an Agilent N5245A PNA-X network analyzer and on-wafer calibration standards. The noise figure and linearity of the active circuits were measured up to 26.5 GHz using the PNA-X. The dual-LNA MMIC designs (see Figure 3) each consist of two-stage GaAs amplifier circuits designed with respect to low NF (LNA1) and high linearity (LNA2), respectively, and that were simulated using foundry-provided design-kit libraries in *ADS* [15]. The dual-LNA MMIC was fabricated using OMMIC's 0.13 μm gate length high electron mobility transistor (HEMT) technology with $f_T = 100$ GHz and $f_{\max} = 180$ GHz. The following gate widths (W_{gi}, $i = 1, 2$) were used within each (two-stage) LNA subcircuit: $W_{g1} = 4 \times 33\,\mu$m, $W_{g2} = 4 \times 29\,\mu$m (LNA1) and $W_{g1} = 8 \times 55\,\mu$m, $W_{g2} = 8 \times 75\,\mu$m (LNA2).

Measured and simulated *s*-parameters and NF of the dual-LNA MMIC (shown in Figure 3 to the right) are shown in Figures 5 and 6, respectively. As can be seen, a relatively good agreement exists between the measured and simulated small-signal data of the two characterised LNA1 and LNA2 break-out circuits that consume 123 mW and 690 mW of P_{DC}, respectively. LNA1 and LNA2 were designed to reach their optimum performance with respect to maximum gain/linearity and lowest possible NF at around 20–25 GHz (i.e., 2-3 dB of NF together with 10–18 dB of in-band gain). The two LNAs further present an output-referred third-order intercept point (OIP_3) and an output 1 dB compression point ($P_{1\,\mathrm{dB}}$) in the order of 20–30 dBm and 10–20 dBm at 18–26 GHz, respectively, (see Figure 7).

2.2. RF-MEMS Reconfigurable (Multifunctional) K-Band LNA. Figure 8 shows measured *s*-parameters (3-port) of the reconfigurable dual-path LNA hybrid circuit (shown in Figure 3) when the RF-MEMS switches used in the two branches were switched ON and OFF, respectively. When the LNA1 path was activated (MEMS switched ON), the other

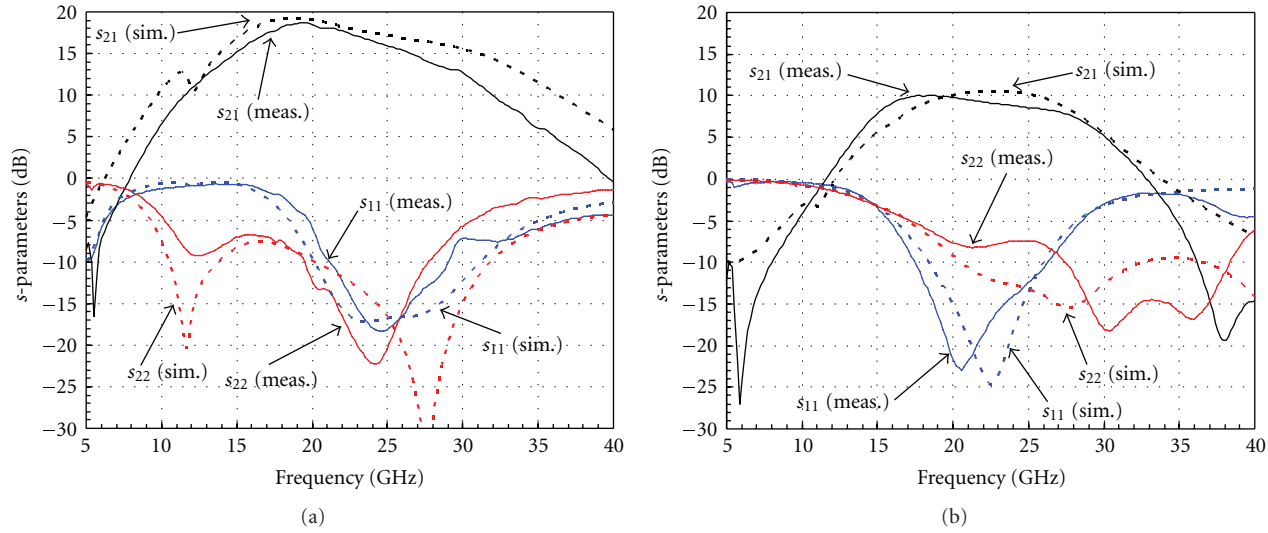

FIGURE 5: Measured and simulated s-parameters of the dual-LNA MMIC with subcircuits LNA1 (a) and LNA2 (b) designed for low NF and high linearity, respectively.

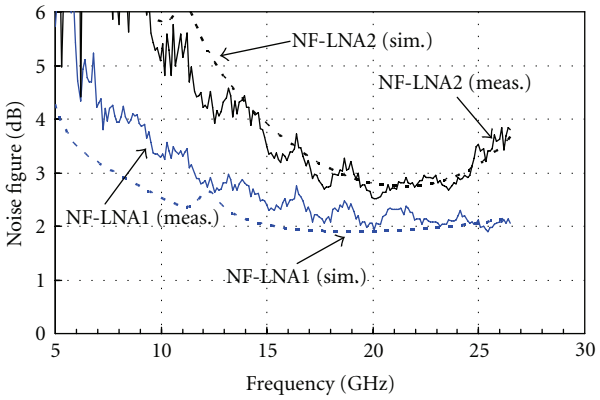

FIGURE 6: Measured and simulated NF of the dual-LNA MMIC with subcircuits LNA1 and LNA2 designed for low NF and high linearity, respectively.

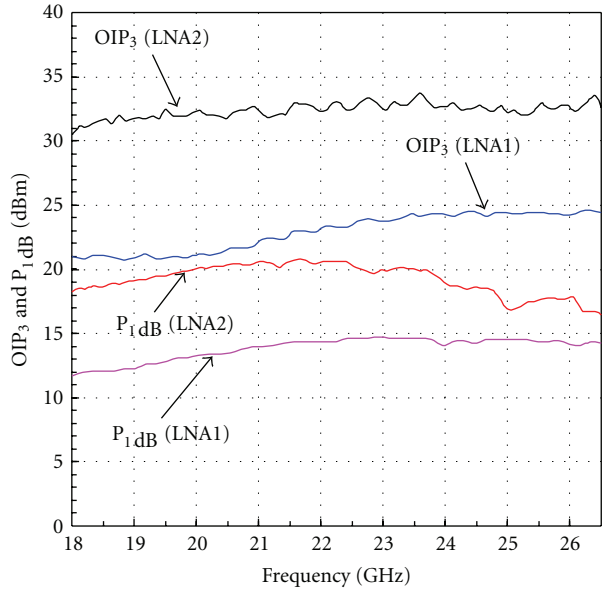

FIGURE 7: Measured $P_{1\,dB}$ and OIP_3 of the dual-LNA MMIC with subcircuits LNA1 and LNA2 designed for low NF and high linearity, respectively.

LNA2 path was deactivated (MEMS switched OFF) and vice versa. In this case, only one of the two individual (fixed) LNA circuits (LNA1 or LNA2) was DC biased at the time to minimise P_{DC}.

When LNA1 was selected (LNA2 OFF), a maximum s_{21} of 16.9 dB was reached at 19.4 GHz (see Figure 8(a)). In this case, the MEMS switched dual-LNA hybrid circuit was well matched at 22–25 GHz (with s_{11}, s_{22}, s_{21}, and s_{31} equal to −28.6 dB, −31.2 dB, 16.3 dB, and −11.6 dB at 23.7 GHz, resp.). The results when LNA2 was selected (LNA1 path deactivated) are shown in Figure 8(b) (s_{11}, s_{22}, s_{21}, and s_{31} equal to −10.8 dB, −8.0 dB, 8.3 dB, and −21.0 dB at 23.7 GHz, resp.). Measured values of s_{21} for the switched LNA1 and LNA2 paths are 1-2 dB lower compared with the corresponding measured gain values of the two (fixed) LNAs (see Figure 5). For the switched LNA1 and LNA2 paths the difference between the measured ON/OFF state LNA gain (i.e., $s_{21} - s_{31}$ in dB) is around 28-29 dB at 23.7 GHz, respectively.

Figures 9(a) and 9(b) show measured NF and $P_{1\,dB}$ of the K-band (18–26.5 GHz) MEMS-switched reconfigurable dual-path LNA hybrid circuit for one of the two LNA1/LNA2 paths that was switched ON at a time (the other LNA path was switched OFF and the LNA in that branch was also either unbiased or biased). The NF of the switched LNA1 and LNA2 paths (with LNA2/LNA1 unbiased) equals 2.7–3.4 dB and 4.1–5.1 at 18.0–25.0 GHz, respectively (3.2–3.8 dB and 4.2–5.3 dB with LNA2/LNA1 also biased). Within this frequency band, measured values of NF for the MEMS-switched LNA1/LNA paths (with the other LNA unbiased) are 1-2 dB higher than that of the individual (fixed) LNA1

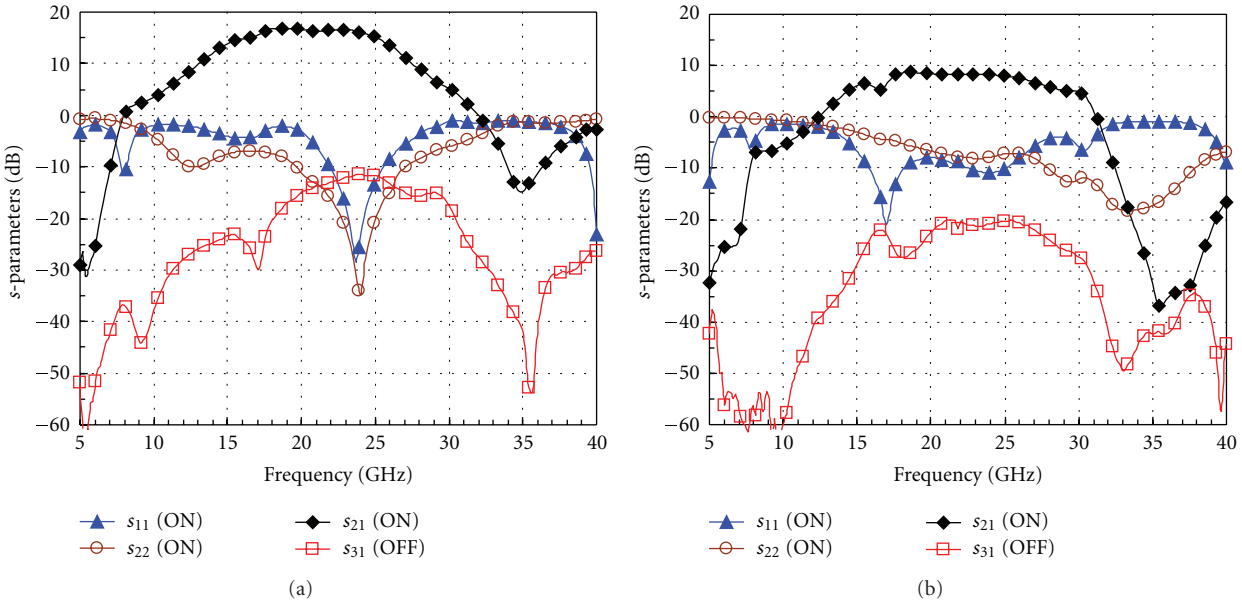

FIGURE 8: Measured *s*-parameters of the RF-MEMS reconfigurable (multifunctional) dual-path LNA hybrid circuit: (a) LNA1 switched ON (LNA2 OFF) and (b) LNA2 switched ON (LNA1 OFF).

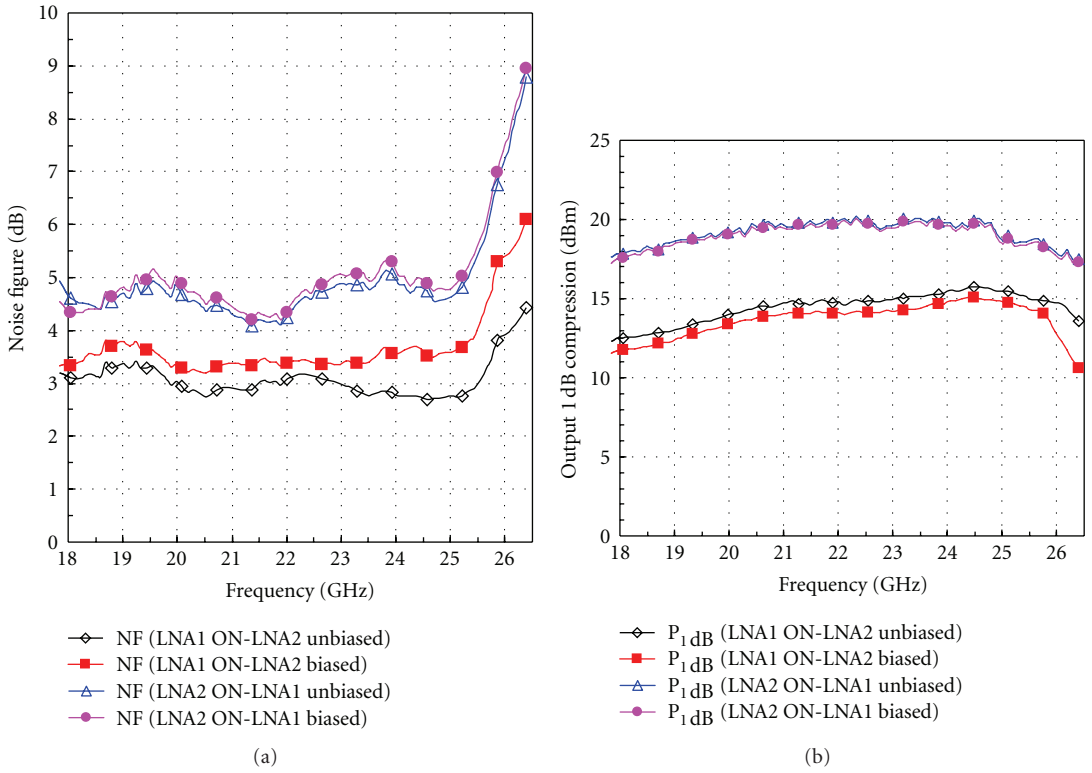

FIGURE 9: Measured NF (a) and $P_{1\,\mathrm{dB}}$ (b) of the MEMS reconfigurable LNA (hybrid circuit) for one of the two LNA paths that was switched ON (while the other LNA path was switched OFF and the LNA in that branch was also either unbiased or biased).

and LNA2 circuits, respectively (NF = 1.9–2.5 dB and 2.5–3.5 dB at 18.0–25.0 GHz). The slightly higher measured in-band NF (and also lower gain) of the switched dual-LNA hybrid circuit (compared with the LNA1/LNA2 MMICs used here as subcircuits) can be attributed to the insertion loss of the MEMS SPDT switch network, losses within the interconnecting bond wires and mismatching. The large-signal characterisation shows measured (in-band) values of $P_{1\,\mathrm{dB}}$ for the MEMS-switched dual-LNA that are close to the corresponding data of the LNA1 and LNA2 circuits,

Table 1: Results of RF-MEMS-Switched LNAs and fixed LNAs.

Circuit/RF performance (at 24 GHz)	Gain (ON) (dB)	Gain (OFF) (dB)	NF (dB)	$\mathbf{P_{1\,dB}}$ (dBm)
SPDT (type I)	−1.4	−13.0	1.4 (estim.)	N/A
SPDT (type II)	−0.9	−22.0	0.9 (estim.)	N/A
LNA1 (low NF)	17.0	N/A	2.2	14
LNA2 (high linearity)	9.5	N/A	2.9	19
Switched LNA1 (low NF)	16.0	−11.5	2.8	15
Switched LNA2 (high linearity)	8.2	−20.8	4.9	20

respectively (see Figures 7 and 9(b)). Thus, the linearity of the tested switched LNA is found to be limited by the active devices used and not by the RF-MEMS switches utilised here as switching elements (see also [13]).

Experimental results (at 24 GHz) of the RF-MEMS reconfigurable/multifunctional dual-LNA hybrid circuit (together with corresponding data of the MEMS SPDT and LNA MMIC subparts) are summarised in Table 1. Compared with the LNA1 and LNA2 data, measured values of (in-band) NF (and gain) for the two MEMS-switched LNA1 and LNA2 paths are 0.6–2.0 dB higher (1.0–1.3 dB lower), respectively. The somewhat less increased NF (and also reduced gain) for the switched LNA1 path can be explained by the fact that it is better matched than the switched LNA2 path (s_{11} equals −22 dB/−10 dB at 24 GHz, resp.). The experimental results presented in this paper demonstrate the feasibility of realising a wire-bonded K-band (18–26.5 GHz) RF-MEMS reconfigurable dual-LNA hybrid circuit optimised for different RF functions such as low NF and high linearity, respectively.

3. Conclusion

We presented a K-band (18–26.5 GHz) RF-MEMS reconfigurable and multifunctional dual-path LNA (optimised for lowest/highest possible NF/linearity, resp.) which has been realised as a hybrid circuit with a total circuit size equal to $3 \times 5\,\text{mm}^2$. Compared with the (fixed) LNA subcircuits used, the two wire-bonded MEMS-switched LNA circuit functions (paths) show minimum 0.6–1.3 dB higher NF (1-2 dB lower gain) and similar linearity levels at 18–25 GHz. The small-signal gain of one of the two reconfigurable LNA circuit paths is reduced by 25–30 dB when the MEMS switch and active circuitry used within the same switching branch are switched off to select the other LNA path and minimise power consumption. The K-band dual-LNA circuit presented in this paper is believed to be the first reported RF-MEMS reconfigurable multifunctional (low-noise and high-linearity) amplifier with NF = 3–5 dB and $P_{1\,\text{dB}}$ = 12–20 dBm at 18–25 GHz. Such low-noise, low-power and high-linearity, high-gain MEMS reconfigurable active RF circuits can enable highly adaptive high performance wideband/multiband front-ends up to the mm wave range.

Acknowledgments

The authors wish to acknowledge the European Union for the funding and support of the FP7 project MEMS-4-MMIC (Grant Agreement no. 224101), VINNOVA and TEKES for the funding and support of the NORDITE project MOSART (Grant Agreement no. 2007-01975 and 40266/07). The work was also carried out in the framework of COST Action IC-0803-RF/Microwave Communication Subsystems for Emerging Wireless Technologies (RFCSET).

References

[1] TGS8250-SCC, Product Data Sheet, 2001, http://www.triquint.com.

[2] TGS2302, Product Data Sheet, 2008, http://www.triquint.com.

[3] RMSW221, Product Data Sheet, 2011, http://www.radant-mems.com.

[4] M. Kim, J. B. Hacker, R. E. Mihailovich, and J. F. DeNatale, "A monolithic MEMS switched dual-path power amplifier," *IEEE Microwave and Wireless Components Letters*, vol. 11, no. 7, pp. 285–286, 2001.

[5] J. B. Hacker, M. Kim, R. E. Mihailovich, and J. F. DeNatale, "Monolithic GaAs PHEMT MMICs integrated with RF MEMS switches," in *Proceedings of the IEEE Compound Semiconductor Integrated Circuit Symposium*, pp. 229–232, October 2004.

[6] D. Qiao, R. Molfino, S. M. Lardizabal, B. Pillans, P. M. Asbeck, and G. Jerinic, "An intelligently controlled RF power amplifier with a reconfigurable MEMS-varactor tuner," *IEEE Transactions on Microwave Theory and Techniques*, vol. 53, no. 3, pp. 1089–1095, 2005.

[7] M. Liu, M. Libois, M. Kuijk, A. Barel, J. Craninckx, and B. Come, "MEMS-enabled dual-band 1.8 & 5-6 GHz receiver RF front-end," in *Proceedings of the IEEE Radio and Wireless Symposium*, pp. 547–550, January 2007.

[8] T. Mukherjee and G. K. Fedder, "RF-CMOS-MEMS based frequency-reconfigurable amplifiers," in *Proceedings of the IEEE Custom Integrated Circuits Conference*, pp. 81–84, September 2009.

[9] H. Okazaki, K. Kawai, A. Fukuda, T. Furuta, and S. Narahashi, "Reconfigurable amplifier towards enhanced selectivity of future multi-band mobile terminals," in *Proceedings of the IEEE International Microwave Workshop Series on RF Front-ends for Software Defined and Cognitive Radio Solutions (IMWS' 10)*, pp. 15–18, February 2010.

[10] K. Joshin, Y. Kawano, X. Mi et al., "K-band CMOS-based power amplifier module with MEMS tunable bandpass filter," in *Proceedings of the 13th European Integrated Circuits Conference*, pp. 440–443, September 2010.

[11] E. Evans, J. C. Rock, T. Hudson et al., "Iteration of a MEMS-based, Ka-band, 16-element sub-array," in *Proceedings of the IEEE Aerospace Conference*, pp. 1–13, March 2011.

[12] R. Liu, D. Schreurs, W. De Raedt, F. Vanaverbeke, and R. Mertens, "RF-MEMS based tri-band GaN power amplifier," *Electronics Letters*, vol. 47, no. 13, pp. 762–763, 2011.

[13] TGS8250-SCC, Product Data Sheet, February, 2001, http://www.triquint.com.
[14] R. Malmqvist, C. Samuelsson, W. Simon et al., "Reconfigurable wideband LNAs using ohmic contact and capacitive RF-MEMS switches," in *Proceedings of the 6th European Microwave Integrated Circuits Conference*, October 2011.
[15] http://www.ommic.com.